231690

UCRL-JC-127980 Part I
PREPRINT

Crevice Corrosion & Pitting of High-Level Waste Containers: Integration of Deterministic & Probabilistic Models

Joseph C. Farmer
R. Daniel McCright

This paper was prepared for submittal to the
National Association of Corrosion Engineers Corrosion '98 Meeting
San Diego, CA
March 22-27, 1998

October 1997

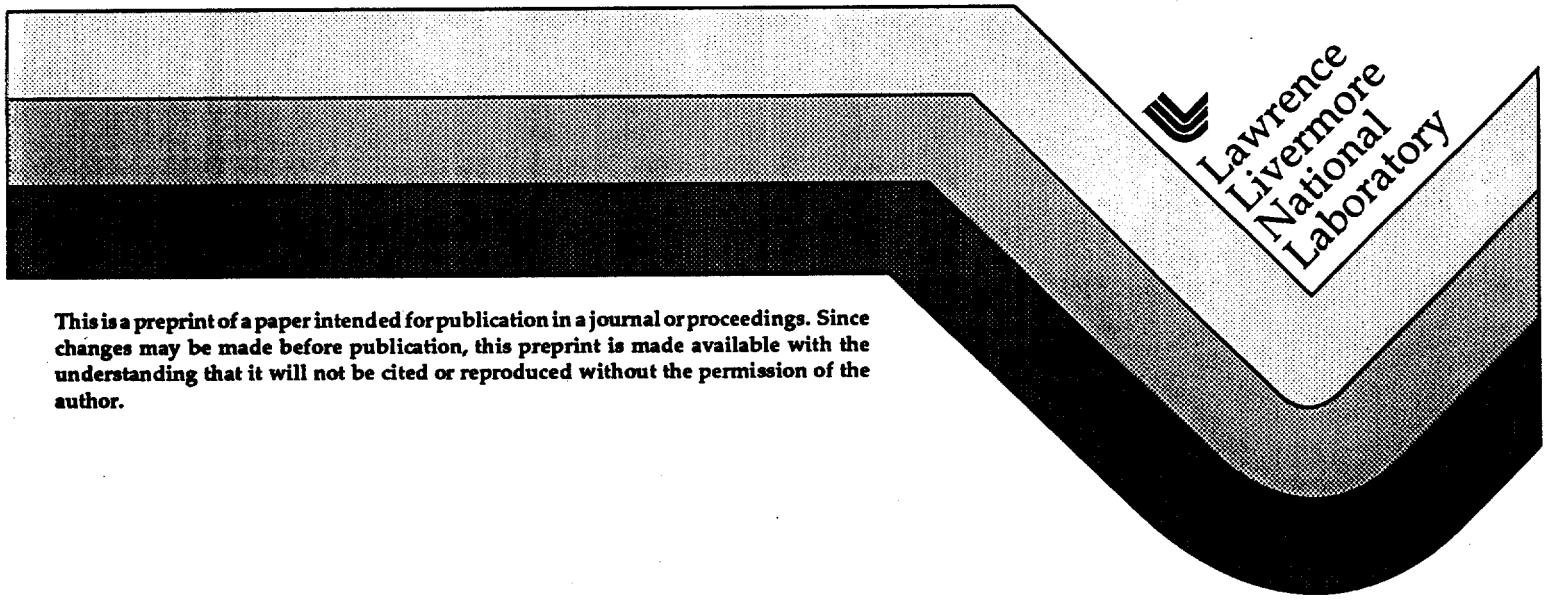

CREVICE CORROSION & PITTING OF HIGH-LEVEL WASTE CONTAINERS: INTEGRATION OF DETERMINISTIC & PROBABILISTIC MODELS

Joseph C. Farmer and R. Daniel McCright
Lawrence Livermore National Laboratory
Livermore, California 94550

ABSTRACT

A key component of the Engineered Barrier System (EBS) being designed for containment of spent-fuel and high-level waste at the proposed geological repository at Yucca Mountain, Nevada is a two-layer canister. In this particular design, the inner barrier is made of a corrosion resistant material (CRM) such as Alloy 625 or C-22, while the outer barrier is made of a corrosion-allowance material (CAM) such as carbon steel or Monel 400. An integrated predictive model is being developed to account for the effects of localized environmental conditions in the CRM-CAM crevice on the initiation and propagation of pits through the CRM.

Key words: crevice corrosion, pitting, model, high-level waste, Alloy 625 and Alloy C-22

INTRODUCTION

A key component of the Engineered Barrier System (EBS) being designed for containment of spent-fuel and high-level waste at the proposed geological repository at Yucca Mountain, Nevada is a two-layer canister. In this particular design, the inner barrier is made of a corrosion resistant material (CRM) such as Alloy 625 or C-22, while the outer barrier is made of a corrosion-allowance material (CAM) such as carbon steel or Monel 400. Initially, the containers will be hot and dry due to the heat generated by radioactive decay. However, eventually the temperature will drop to levels where both humid air and aqueous phase corrosion will be possible. As the outer barrier is penetrated, the possibility for crevice formation between the CAM and CRM will exist. In the case of Alloys 625 and C-22, it is evident that a crevice will have to form before significant penetration of the CRM can occur. Integrated predictive models are being developed to account for the effects of localized environment in the crevice on pit initiation and propagation. For example, a deterministic calculation is used to estimate the concentration of accumulated hydrogen ions (pH suppression) in the crevice due to hydrolysis reactions of dissolved iron, nickel and chromium. Sufficient chloride must then be transported into the crevice by diffusion and electromigration to satisfy conditions of electroneutrality. Pit initiation and growth within the crevice is then dealt with by either a probabilistic model, or an equivalent deterministic model. The deterministic model is based upon simultaneous integration of the rate

expressions for pit embryo formation, the rate of stable pit formation from embryos, and the time-dependent rate of pit propagation.

A plausible scenario has been developed. First, penetration of the outer barrier (CAM) will occur due to humid air corrosion or aqueous corrosion. The inner barrier (CRM) will then be exposed in patches, with formation of a crevice between the CAM and CRM. Crevice regions surrounding the exposed patches can be subdivided into three types of generic zones. *Zone 1:* areas where the CRM will be directly exposed to the NFE, via humid air or a thin layer of oxygenated and acidified water. *Zone 2*: areas where the CRM will be exposed to a thin layer of acidified water, with a gradient in oxygen concentration. *Zone 3*: areas where the CRM will be exposed to a thin layer of acidified and deoxygenated water. The corrosion phenomena in these zones may progress through two distinct phases. *Phase 1*: general corrosion of the crevice wall formed by the CAM. *Phase 2*: localized corrosion of the crevice wall formed by the CRM. The three generic zones are illustrated in Figure 1.

The crevice corrosion of Alloy 625 under conditions similar to those expected during Phase 2 has been well documented. For example, Lillard and Scully have induced crevice corrosion in chlorinated ASTM artificial sea water and documented the attack with photographs [1]. Asphahani has observed that the corrosive dissolution rates of several high-performance alloys, including Alloy 625, are accelerated in $FeCl_3$ solutions [2,3]. Frequently, $FeCl_3$ solutions are used to simulate the harsh conditions found in crevices. Jones and Wilde have prepared solutions of $FeCl_2$, $NiCl_2$ and $CrCl_3$, and measured substantial pH suppression [4]. Under such harsh conditions, one would expect enhanced rates of pit initiation and propagation, as well as intergranular corrosion. In less severe conditions without $FeCl_3$, no significant attack has been observed [5,6].

In regard to Total System Performance Analysis (TSPA) of the repository proposed for construction at Yucca Mountain, it is prudent to account for the harsh localized environment that may exist in the crevice separating the inner and outer barriers. A relatively detailed deterministic crevice model has been developed to calculate: (a) potential and current distributions; (b) local penetration rates; and (c) transient concentrations of various species. Concentration profiles predicted by the model include those of: dissolved oxygen; dissolved iron, nickel, chromium, and molybdenum; hydrogen ions generated by the hydrolysis of dissolved metal ions; and aggressive anions such as chloride. The accumulation of H^+ in the crevice will cause significant suppression of the pH. Since electroneutrality must be maintained, sufficient Cl^- must be transported into the crevice to balance the charge of accumulated hydrogen ions. These interfacial effects will "set the stage" for localized attack of the CRM by pitting and intergranular corrosion. Reasonable estimates of H^+ and Cl^- concentrations in the CAM-CRM crevice have facilitated application of other corrosion models at this boundary, including a probabilistic pitting model which has been used to predict the nucleation and growth of pits on the CRM during Phase 2. This model is similar to those discussed by Shibata [7,8] and Henshall [9-11]. However, enhancements were needed to enable the calculations to account for the effects of pH on pitting.

CREVICE CORROSION MODEL

Crevice Chemistry

As discussed by Oldfield and Sutton, metal ions produced by anodic dissolution are assumed to undergo the following hydrolysis reactions [12]:

$$Fe^{2+} + H_2O \underset{K_{3,1}}{\longleftrightarrow} Fe(OH)^{+} + H^{+} \quad (1)$$

$$Fe^{3+} + H_2O \underset{K_{4,1}}{\longleftrightarrow} Fe(OH)^{2+} + H^{+} \quad (2)$$

$$Ni^{2+} + H_2O \underset{K_{5,1}}{\longleftrightarrow} Ni(OH)^{+} + H^{+} \quad (3)$$

$$Cr^{3+} + H_2O \underset{K_{1,1}}{\longleftrightarrow} Cr(OH)^{2+} + H^{+} \quad (4)$$

$$Cr(OH)^{2+} + H_2O \underset{K_{1,2}}{\longleftrightarrow} Cr(OH)_2^{+} + H^{+} \quad (5)$$

Relevant equilibrium constants are defined as follows [12,13]:

$$K_{3,1} = \frac{\left[Fe(OH)^{+}\right]\left[H^{+}\right]}{\left[Fe^{2+}\right]} \quad (6)$$

$$K_{4,1} = \frac{\left[Fe(OH)^{2+}\right]\left[H^{+}\right]}{\left[Fe^{3+}\right]} \quad (7)$$

$$K_{5,1} = \frac{\left[Ni(OH)^{+}\right]\left[H^{+}\right]}{\left[Ni^{2+}\right]} \quad (8)$$

$$K_{1,1} = \frac{\left[Cr(OH)^{2+}\right]\left[H^{+}\right]}{\left[Cr^{3+}\right]} \quad (9)$$

$$K_{1,2} = \frac{\left[Cr(OH)_2^{+}\right]\left[H^{+}\right]}{\left[Cr(OH)^{2+}\right]} \quad (10)$$

If the dissolved metals exceed the solubility limits, precipitation will occur:

$$Fe(OH)_2(s) \underset{K_{3,3}}{\longleftrightarrow} Fe^{2+} + 2OH^{-} \quad (11)$$

$$Ni(OH)_2(s) \xleftrightarrow[K_{5,3}]{} Ni^{2+} + 2OH^- \tag{12}$$

$$Cr(OH)_3(s) \xleftrightarrow[K_{1,3}]{} Cr^{3+} + 3OH^- \tag{13}$$

The corresponding solubility products are:

$$K_{3,3} = \left[Fe^{2+}\right]\left[OH^-\right]^2 \tag{14}$$

$$K_{5,3} = \left[Ni^{2+}\right]\left[OH^-\right]^2 \tag{15}$$

$$K_{1,3} = \left[Cr^{3+}\right]\left[OH^-\right]^3 \tag{16}$$

It is assumed that anodic dissolution reactions are depolarized by the cathodic reduction of dissolved oxygen or hydrogen evolution [14].

Hydrogen Ion Generation Rate

Hydrolysis reactions of various dissolved metal ions will result in pH suppression within the crevice. In order to quantify this effect, it is necessary to account for the net accumulation of hydrogen ions. The corresponding mass balance is:

$$\left[H^+\right] = \left[H^+\right]_{Fe(II)} + \left[H^+\right]_{Fe(III)} + \left[H^+\right]_{Ni(II)} + \left[H^+\right]_{Cr(III)} - \left[H^+\right]_{H_2} - \left[H^+\right]_{O_2} \tag{17}$$

In the present model, the effects of hexavalent chromium and molybdenum on pH are assumed to be insignificant. The quantity of hydrogen ions generated by the hydrolysis of divalent iron ions produced during the dissolution of either the CAM or CRM is:

$$\left[H^+\right]_{Fe(II)} = 2\left[Fe(OH)_2\right](s) + \left[Fe(OH)^+\right] \tag{18}$$

The dissolved Fe^{2+} can be converted to Fe^{3+} by: (I) microbial action; (ii) oxidation by naturally occurring MnO_2 or other oxidants; or (ii) anodic oxidation. Once formed, it is assumed that Fe^{3+} can also undergo hydrolysis. The quantity of hydrogen ions produced by this reaction is:

$$\left[H^+\right]_{Fe(III)} \approx \left[Fe(OH)^{2+}\right] \tag{19}$$

Dissolution of the CRM will produce divalent nickel and trivalent chromium ions, in addition to divalent iron ions. The equations for the divalent nickel are analogous to those for the divalent iron:

$$\left[H^+\right]_{Ni(II)} = 2\left[Ni(OH)_2\right](s) + \left[Ni(OH)^+\right] \tag{20}$$

The equations for the trivalent chromium are similar to those for the trivalent iron:

$$\left[H^+\right]_{Cr(III)} = 3\left[Cr(OH)_3\right](s) + 2\left[Cr(OH)_2^+\right] + \left[Cr(OH)^{2+}\right] \tag{21}$$

Hydrogen ions lost due to hydrogen evolution and the cathodic reduction of oxygen are represented by:

$$\left[H^+\right]_{H_2} = 2\left[H_2\right] \tag{22}$$

$$\left[H^+\right]_{O_2} = 4\left[O_2\right] \tag{23}$$

Equations 18 through 23 are substituted into Equation 17. The concentrations of soluble hydrolysis products are then expressed in terms of $[H^+]$ and the concentrations of unhydrolyzed metal ions. The result is then differentiated with respect to time to yield the following H^+ generation rate:

$$\frac{d\left[H^+\right]}{dt} = \frac{\left\{\frac{K_{3,1}}{\left[H^+\right]}\frac{d\left[Fe^{2+}\right]}{dt} + \frac{K_{4,1}}{\left[H^+\right]}\frac{d\left[Fe^{3+}\right]}{dt} + \frac{K_{5,1}}{\left[H^+\right]}\frac{d\left[Ni^{2+}\right]}{dt} + \frac{K_{1,1}}{\left[H^+\right]}\frac{d\left[Cr^{3+}\right]}{dt} + \frac{2K_{1,1}K_{1,2}}{\left[H^+\right]^2}\frac{d\left[Cr^{3+}\right]}{dt} - 2\frac{d\left[H_2\right]}{dt} - 4\frac{d\left[O_2\right]}{dt}\right\}}{\left\{1 + \frac{K_{3,1}\left[Fe^{2+}\right]}{\left[H^+\right]^2} + \frac{K_{4,1}\left[Fe^{3+}\right]}{\left[H^+\right]^2} + \frac{K_{5,1}\left[Ni^{2+}\right]}{\left[H^+\right]^2} + \frac{K_{1,1}\left[Cr^{3+}\right]}{\left[H^+\right]^2} + \frac{4K_{1,1}K_{1,2}\left[Cr^{3+}\right]}{\left[H^+\right]^3}\right\}}$$

The consumption of H^+ by hydrogen evolution and cathodic oxygen reduction is accounted for. Since the H^+ generation rate approaches zero as [H+] and the concentrations of unhydrolyzed metal ions approach infinity (large values), the extent of pH suppression in the crevice is limited. If solubility limits are exceeded, $Fe(OH)_2$, $Ni(OH)_2$ and $Cr(OH)_3$ precipitates are assumed to form. Under these conditions, the H^+ generation rate is proportional to the rates of precipitation, which are directly related to the rates of dissolution. The hydrolysis equilibrium constants can be found in the literature [12,13].

An alternative strategy can be used to estimate pH suppression in the crevice. In this case, it is assumed that acidification of the crevice solution is limited by the transport of Cl^- into the crevice, instead of being limited by H^+ generation and transport out of the crevice. As discussed by Pickering and others, Cl^- will be driven into the crevice by the potential gradient. After the Cl^- concentration is established, the H^+ concentration can be determined with the equation for electroneutrality. The roots of the resulting polynomial in $[H^+]$ determine the pH.

Transient Concentrations

Attention is now directed to transport in the crevice separating the CAM and CRM. As discussed by Newman, fluxes of ions are estimated with the Nernst-Planck equation, which governs electromigration, diffusion, and convective transport [15]:

$$\overline{N}_i = -z_i u_i F c_i \overline{\nabla}\Phi - D_i \overline{\nabla} c_i + v c_i \quad (24)$$

where N_i is the flux, z_i is the charge, u_i is the mobility, c_i is the concentration and D_i is the diffusivity of the i-th ion; Φ is the potential in the electrolyte; and v is the convective velocity of the electrolyte. The current density is then defined in terms of the flux:

$$\bar{i} = -F^2 \overline{\nabla}\Phi \sum_i z_i^2 u_i c_i - F \sum_i z_i D_i \overline{\nabla} c_i \quad (25)$$

In cases with strong supporting electrolyte, the electromigration term can be ignored. Transients in concentration can be dealt with through application of Equation 26:

$$\frac{\partial c_i}{\partial t} = -\overline{\nabla} \cdot \overline{N}_i + R_i \quad (26)$$

where R_i is the (apparent) homogeneous rate. Note that the concentration of dissolved iron is assumed to include all dissolved species, including Fe^{2+}, Fe^{3+}, $Fe(OH)^+$ and $Fe(OH)^{2+}$. Similar assumptions are made for other dissolved metals. The hyperbolic partial differential equations (PDEs) that describe the transport of such reactive species in the crevice can be solved numerically. Both the Crank-Nicholson and the 'explicit' methods have been used [16,17]. The assumed BCs imply that the concentrations are zero at the crevice mouth (NFE), and that crevices are symmetric about a mirror plane where the flux is zero. The BCs for H^+ and dissolved O_2 are slightly different in that non-zero concentrations are assigned at the crevice mouth.

Current and Potential

The PDEs that define transient concentrations in the crevice require determination of the potential gradient, as well as the (apparent) homogeneous rates. First, the axial current density along the length of the crevice, $i_x(x)$, is calculated by integrating the wall current density, $i_y(x)$:

$$i_x(x) = \frac{\int_x^L i_y(x)\,dx}{h(x)} \quad (27)$$

where L is the maximum crevice depth and h(x) is the separation between the two crevice walls at position (x). The electrode potential along the length of the crevice, E(x), can then be calculated from $i_x(x)$:

$$E(x) = \int_0^x \rho(x)\, i_x(x)\,dx \quad (28)$$

where $\rho(x)$ is the resistivity of the crevice solution at position (x). This technique is very similar to that employed in other published models [18-20].

PITTING MODELS

Published Models

Crevice corrosion will result in acidification of the electrolyte and a corresponding elevation in Cl^- concentration. This harsh localized environment may cause pitting, as well as intergranular corrosion. Several pitting models have been reviewed in detail by the author [21]. Those for pit initiation include: the halide nuclei theory by Okada [22,23]; the point defect model by Chao, Lin and McDonald [24]; the electrostriction model by Sato [25]; and the stochastic probability model by Shibata [7,8]. Models for pit propagation include: the Pickering-Frankenthal model [26], which assumes passive walls and an active base; the Galvele modification of the Pickering-Frankenthal model [27], which accounts for the effects of metal ion hydrolysis on pH suppression; and the Beck-Alkire model, which deals with a hemispherical pit covered by a thin, resistive halide film [28]. Henshall was the first to apply probabilistic pitting models to the performance assessment of high-level waste containers [9-11].

Probabilistic Pitting Model

The probabilistic model developed here for pitting of the CRM divides the container surface into a two-dimensional (2D) array of hypothetical cells, where probabilities for the transition from one pitting state to another can be assigned [29]. Nucleation or death of a pit embryo is determined by comparing random numbers, generated by a power residue method, to an environment-dependent birth or death probability, respectively. After a pit embryo reaches a critical age, it is assumed to become a stable pit. This approach has already been explored for modeling pit initiation and growth on high-level waste containers by Henshall [9-11]. However, the Henshall model requires additional work to enable it to deal with important environmental parameters, such as pH. This model assumes that the birth and death probabilities are functions of potential, chloride concentration, and temperature alone. More specifically, the effect of pH is not accounted for. Furthermore, it is necessary to assume that the birth probability decays exponentially with time in order to obtain a reasonably shaped distribution of pit depths, the number of pits verses depth. Ideally, the birth rate (or birth probability) should be time invariant in such a mechanistic model. Finally, the functions used for calculating the birth and death probabilities could have values much greater than unity (>>1), though the code limited the values to one (≤ 1). It is better to use probability expressions where all calculated values lie between zero and one, as done by Shibata [8]. This feature has now been incorporated into the probabilistic pitting model described here. Based upon empirical observations regarding the roles of Cl^- and $E\text{-}E_{crit}$ on pit initiation (birth), as well as empirical observations regarding the roles of OH^- and $E\text{-}E_{pass}$ on repassivation (death), the following equations are assumed for the rates of embryo birth and death:

$$\lambda_1 = \lambda_0 \left[Cl^-\right] \exp\left(\frac{\alpha_\lambda F}{RT}\left(E - E_{crit}\right)\right) \tag{29}$$

$$\mu_1 = \mu_0 \left[OH^-\right] \exp\left(-\frac{\alpha_\mu F}{RT}\left(E - E_{pass}\right)\right) \tag{30}$$

where [Cl$^-$] is the concentration of the chloride anion; [OH$^-$] is the concentration of the hydroxyl anion; F is Faraday's constant; R is the universal gas constant; T is the absolute temperature; E is the electrochemical potential applied to the surface; E_{crit} is the critical pitting potential; E_{pass} is the repassivation potential; α_λ and α_μ are constants; and λ_0 and μ_0 are intrinsic rate constants for the birth and death of embryos, respectively. It is evident that the proposed model involves competitive adsorption of Cl$^-$ and OH$^-$, which is consistent with the discussion by Strehblow and others [30]. The rate of converting an embryo into a stable pit is defined here as the transition rate, γ_1. This conversion process is assumed to be thermally activated and governed by the Ahrenius rate law.

$$\gamma_1 = \gamma_0 \exp\left(-\frac{A_\gamma}{RT}\right) \tag{31}$$

where A_γ is the apparent activation energy and γ_0 is the intrinsic rate constant. In lieu of a transition rate, an induction or incubation time can be used. The induction time, τ_1, is the age that an embryo must reach before it can become a stable pit. This quantity is also assumed to obey an Ahrenius-like expression.

$$\tau_1 = \tau_0 \exp\left(-\frac{A_\tau}{RT}\right) \tag{32}$$

where A_τ is the apparent activation energy and τ_0 is the intrinsic induction time. As described by Shibata [Eqns. 63 & 64, Ref. 8], the birth probability in a single cell ($0 < \lambda < 1$) is calculated from the rate as follows.

$$\lambda = 1 - e^{-\lambda_1 \delta t} \tag{33}$$

The death and transition probabilities are calculated in a similar manner.

$$\mu = 1 - e^{-\mu_1 \delta t} \tag{34}$$

$$\gamma = 1 - e^{-\gamma_1 \delta t} \tag{35}$$

At a given time step, an embryo will be born in a vacant cell if the following criteria are met:

$$RND \le \lambda \tag{36}$$

where RND is a random number. The random number embodies the stochastic nature of pitting events on the surface. Similarly, an existing embryo will die if:

$$RND \le \mu \tag{37}$$

An embryo will become a stable pit if one of the following criteria are met:

$$RND \le \gamma \tag{38}$$

$$\tau_{age} \ge \tau_1 \tag{39}$$

where τ_{age} is the age of the embryo under consideration. It was recognized by Henshall that it is necessary to let the birth probability decay with time to obtain a symmetric distribution of pits centered at the mean pit depth. However, model parameters such as the birth probability should be time invariant. An expression for the birth probability is proposed that accomplishes the same end as Henshall's formulation, and avoids explicit use of time as an independent variable.

$$\lambda = \lambda\left(A\,\theta_P^{\,n} \exp\left[-B\,\theta_P\right]\right) \tag{40}$$

where A and B are constants, θ_P is the fractional coverage of the surface by stable pits, and n is the exponent of θ_P. The ability of such "shape factors" to mimic observed pit distributions may be related to implicit memory effects recognized by Scully and others [31]. Determination of the distribution of pit depths requires calculation of the pit penetration, d, which is a function of pit age, T_{age}. The corresponding penetration rate can be assumed to be limited by either diffusion or electromigration. Both cases yield a square-root dependence of the pit depth on time. Diffusion-limited penetration will be discussed briefly in the following section. Here, for the sake of illustration, the penetration is assumed to obey the following empirical expression:

$$d = \sqrt{2\,K\,T_{age}} \tag{41}$$

where the rate constant, K, is defined as:

$$K = K_0\left[H^+\right]\left(E - E_{crit}\right) \tag{42}$$

where K_0 is a constant; $[H^+]$ is the hydrogen ion concentration; E is the applied voltage; and E_{crit} is the critical pitting potential. It should be noted that this expression implies growth driven by the electric field. Future pitting calculations should use assumptions that are more consistent with those implicit in the crevice model, such as the assumption of a strong supporting electrolyte. It must be noted that the pit can "die" if the depth becomes so great that the current density at the base of the pit falls below the passive current density. The importance of such "stifling" has also been pointed out by Scully [31]. In the case of pit propagation in carbon steel, Marsh gives the following criteria based upon the passive current density, i_{pass} [32]:

$$\frac{i_{pass}}{4F} \le D\left.\frac{\partial C(x,t)}{\partial x}\right|_{x=0} \tag{43}$$

It was noted that careful measurements of i_{pass} are required for any theoretical analysis.

where d_0 is the penetration depth at time t_0, d is the penetration depth at time t, and n is the power of the growth law. The special case with n ~ 1/2 corresponds to the well-known Sand equation, which assumes a diffusion-limited electrochemical process.

Data published by Asphahani [2,3] and compiled by Gdowski [33] has been used to establish the following empirical correlations for Alloys 625 and C-22 in simulated crevice solutions with 10 wt. % $FeCl_3$:

$$\ln(\Psi) = \ln(3.81) - 2.4010\,001 \times 10^{-3}(T - T_0) - 2.3662\,274 \times 10^{-1}(T - T_0)^2 \quad (48)$$

$$\ln(\Psi) = \ln(0.25) - 1.2374\,959 \times 10^{-3}(T - T_0) - 2.9368\,571 \times 10^{-2}(T - T_0)^2 \quad (49)$$

where T is the absolute temperature and T_0 is the reference temperature of 298 K. The parameter Ψ is defined as follows:

$$\Psi = \frac{d}{\sqrt{t}} \quad (50)$$

Equations 48 and 49 and similar correlations for other alloys were used calculate the values of Ψ plotted in Figure 2. Predicted penetrations for Alloys 625 and C-22 at several temperature levels between 20 and 100°C are shown in Figures 3 and 4, respectively. After 10,000 years at 80°C, the predicted penetration of Alloy C-22 does not exceed the thickness of the inner barrier wall (2 cm).

RESULTS

Predicted Environment in Crevice

The Crank-Nicholson method was used to calculate concentration profiles during Phase 1 crevice corrosion, as shown in Figure 5. Soluble iron species included in the calculation were Fe^{2+}, Fe^{3+}, $Fe(OH)^{2+}$ and $Fe(OH)^{+}$. All precipitated iron is assumed to be $Fe(OH)_2$. Furthermore, it is assumed that: (a) the temperature is 90°C or 363 K; the potential at the mouth of the crevice is at +10 mV relative to the corrosion potential of Alloy 516, the assumed CAM; the solution conductivity is 50,000 $\mu S\ cm^{-1}$; and the diffusion coefficient of all dissolved species is approximately $1.0 \times 10^{-5}\ cm^2\ sec^{-1}$. Roy et al. have measured relevant corrosion, pitting and repassivation potentials for Alloys 516, 825, 625 and C-22 [34-36]. Results at 0, 600, 1200, 1800, 2400 and 3000 seconds are presented, though calculations were done at intervals of 1 second. The peak in the iron concentration near the crevice mouth is due to the combined effects of a potential that decays with increasing crevice depth (x), and the assumed BC of zero concentration at the crevice mouth. Results obtained with the explicit method are identical.

Calculations for Phase 2 crevice corrosion of Alloy 625 are shown in Figures 6 through 10. Transients in the total concentration of dissolved iron are shown at 0, 600, 1200, 1800, 2400, 3000 and 3600 seconds. Assumed dissolved metal species included in the calculation are Fe^{2+}, $Fe(OH)^{+}$, Fe^{3+}, $Fe(OH)^{2+}$, Ni^{2+}, $Ni(OH)^{+}$, Cr^{3+}, $Cr(OH)^{2+}$, $Cr(OH)_2^{+}$ and Mo^{3+}. Precipitates are assumed to be $Fe(OH)_2$, $Ni(OH)_2$, $Cr(OH)_3$ and $Mo(OH)_3$. Furthermore, it is assumed that: (a) the temperature is 90°C or 363 K;

the potential at the mouth of the crevice is at +100 mV relative to the pitting potential of Alloy 625, the assumed CRM; the solution conductivity is 1000 μS cm^{-1}; and the diffusion coefficient of all dissolved species is approximately $1.9x10^{-5}$ cm^2 sec^{-1}. Based upon the work of Roy et al., the pitting potential is assumed to be +689 mV vs. SCE. As shown in Figures 6 through 8, the concentrations of dissolved metals rise sharply from zero at the crevice mouth to peak values inside the crevice (~0.3 cm). Recall that the concentrations are assumed to be zero at the crevice mouth. At large distances into the crevice (~0.9 cm), the concentrations fall from the peak values to plateaus. Since H^+ is generated by the hydrolysis of iron, nickel and chromium, and since it is transported in a similar fashion, its transient concentration profiles (not shown) track those of the dissolved metals. Figure 9 shows the pH profiles that correspond to Figures 6 through 8. In this particular case, it is concluded that reasonable pH values for the crevice solution lie between 2.8 and 3.2 during Phase 2. The concentrations of dissolved metal ions and H^+ are used to calculate Cl^- concentration (not shown). Alternatively, the Cl^- concentration could be calculated directly from the potential, as suggested by Pickering and Frankenthal [26], as well as Galvele [27]. As shown in Figure 10, the potential drops to more cathodic values as the distance into the crevice increases. The applied potential at the crevice mouth is assumed to be +1,030 mV vs. NHE (+789 mV vs. SCE). At a depth of 1 cm, the predicted potential is somewhere between +870 and +910 mV vs. NHE (+630 and +670 mV vs. SCE). The oscillations in the potential profiles are due to the antagonistic effects of chloride and potential on the anodic current density at the crevice wall. More specifically, the anodic current due to localized attack is driven by the difference between the electrode potential, E, and the pitting potential, E_{crit}. The pitting potential is assumed to obey the expression given by Galvele [27]:

$$E_{crit} = A - B \ln\left[Cl^-\right]$$

where A and B are constants. Note that B is given as ~88 mV for Fe-18Cr-8Ni in NaCl solutions. As the potential in the crevice decreases, the chloride concentration increases, thereby driving the pitting potential to more cathodic levels (less stability). Thus, the anodic current is simultaneously driven by two opposed forces, increasing chloride and decreasing potential. The axial and wall current densities also exhibit oscillations (not shown). In the future, the data collected by Roy et al. should be used to establish the dependence of E_{crit} on Cl^- concentration [34-36].

Probabilistic Pitting Model.

Figure 11 shows the calculated pit density (cells or number per 100 cm^2) as a function of time, based upon the probabilistic model. As expected, the number of vacancies (unpitted area) decreases with time, while the number of stable pits increases. Initially, the number of pit embryos increases rapidly with time. However, the embryo density reaches a maximum and begins to fall at the point where the rate of embryo conversion to stable pits exceeds the rate of embryo births. The overall pit generation rate is proportional to the embryo density, and also passes through a maximum. Figure 12 shows the corresponding pit distribution, which is typical of those obtained with the stochastic pitting model with time invariant probabilities. Distinguishing characteristics include: peak near the maximum pit depth; and a long tail. These calculations were performed with parametric values shown in Table 1. These values enabled the model to mimic the experimental pit distribution data for Alloy 825 that was collected by Roy and published by Henshall [11]. In Roy's experiment, samples were exposed to 5 wt.

% NaCl solution at a pH of 2.57 and a temperature of 90°C for 240 minutes. A total of 68 pits were observed in an area of approximately 1 cm^2. The mean depth was 0.345 mm, with a maximum pit depth of 0.505 mm. These data are used as a "bench mark" for model development.

Integration of Pitting and Crevice Corrosion Models

The effect of pH suppression on pitting of the CRM was investigated with the probabilistic model. These calculations were also performed with the parametric values given in Table 1. Figure 13 shows transients in the vacancy, embryo and stable-pit densities (cells) that were predicted for two cases, direct exposure to the near field environment (NFE), and exposure to the low-pH crevice solution. In the NFE case, the assumed environment is a 1100 ppm NaCl solution at pH ~7 and 60°C. The CRM is assumed to be polarized at a level slightly above the pitting potential, approximately +90 mV vs. SCE. In the crevice case, the assumed environment is a 2000 ppm NaCl solution at pH ~3 and 60°C. Here too the potential is assumed to be approximatley +90 mV vs. SCE. The number of vacancies (cells without embryos or stable pits) decreases with time in both cases, while the number of stable pits increases. Initially, the number of pit embryos increases rapidly with time. A maximum is reached at the point where the rate of embryo conversion to stable pits (loss) exceeds the rate of embryo births (generation). The overall pit generation rate is proportional to the embryo density, and also passes through a maximum. Clearly, suppressed pH increases the rate of pit generation, which is consistent with experience. The effect of polarization on the pitting of the inner barrier is illustrated by Figure 14. Case A assumes a 1000 ppm TDS NaCl solution at pH ~7, a temperature of 60°C, and an applied potential of -712 mV vs. SCE, which corresponds roughly to the corrosion potential of the CAM. Case B assumes a 2000 ppm TDS NaCl solution at pH ~3, a temperature of 60°C, and a potential of +90 mV vs. SCE, which corresponds roughly to the pitting potential of the CRM. While rapid pitting of the CRM is predicted for Case B, no pitting is predicted in Case A. The model predicts that the corrosion potential of the CAM provides some protection for the inner barrier.

SUMMARY

In regard to the simulated crevice corrosion of Alloy 625, the concentrations of all species dissolved in the crevice solution approach asymptotic values as time increases. Consequently, the pH approaches an ultimate, asymptotic value. The predicted pH of 2.8-3.2 appears to be very reasonable since it is comparable to measured values [4]. This result leads to a very useful conclusion. When treating localized corrosion within the crevice, one can estimate the asymptotic value of pH and use it as an input to other corrosion models. This asymptotic value can serve as the basis for predicting rates of localized attack of the crevice wall formed by the CRM. Clearly, such a simplification would provide great computational advantages for Total System Performance Assessment (TSPA).

In the case of Alloy 825, it is possible to adjust parameters in the probabilistic pitting model to mimic the distribution of pit depths observed by Roy after 240 hours of accelerated testing. However, in order to match the distribution (mean and maximum depths), it is necessary to apply an appropriate "shape factor" to the birth rate. This "shape factor" is a function of the density of stable pits on the surface, and forces the birth rate to pass through a maximum as the pit density increases. This strategy is attractive in that it eliminates time from the expression for birth rate, while providing essentially the same advantage

as the successful formulation given by Henshall [11]. It is demonstrated that no significant pitting is predicted at potentials that are much more cathodic than the critical pitting potential of the CRM. As long as the potential in the crevice is less than or equal to the corrosion potential of the carbon steel CAM, very little pitting of the CRM is predicted.

Two independent pitting models have been formulated, one probabilistic and the other deterministic. Both are capable of giving comparable qualitative results and predict that vacant surface decreases with time as the number of stable pits increases. Both predict that the number of pit embryos passes through a maximum as the rate of death and conversion to stable pits exceeds the rate of birth. A rational dependence on chloride concentration, pH, potential and temperature have now been built into both models so that the effects of pH suppression in the crevice can be accounted for. The deterministic model offers a significant computational advantage for future TSPA efforts.

A solid step has now been taken towards integrating a crevice corrosion and pitting model. However, much more work needs to be done on the mechanistic pitting and crevice corrosion models provided by this report before they can be reliably used to make quantitative predictions for TSPA. In the interim period, empirical rate expressions, based upon experimental data and a general knowledge of such transport-controlled processes, can be used for bounding, worst-case predictions. Based upon such worst-case predictions, it appears that Alloy C-22 has sufficient corrosion resistance to enable the inner barrier to meet design requirements, regardless of the assumptions made in a particular TSPA model. This material could be used as the basis of a conservative design.

ACKNOWLEDGEMENTS

Discussions with D. Stahl, K. McCoy, J. Lee, W. Clarke, W. Halsey, D. McCright, G. Henshall, D. Jones, J. Horne, J. Payer, J. Scully and J. Blink were very helpful. The careful proof-reading and editorial work of N. Poggio is gratefully acknowledged. This work was done under the auspices of the U.S. Department of Energy (DOE) by Lawrence Livermore National Laboratory (LLNL) under Contract No. W-7405-Eng-48.

REFERENCES

1. R. S. Lillard, J. R. Scully, Modeling of the Factors Contributing to the Initiation and Propagation of the Crevice Corrosion of Alloy 625, J. Electrochem. Soc., Vol. 141, No. 11, 1994, pp. 3006-3015.

2. Haynes International, Inc., Hastelloy Alloy C-276, Haynes Product Brochure H-2002B, Haynes International, 1987.

3. A. I. Asphahani, Corrosion Resistance of High Performance Alloys, Materials Performance, Vol. 19, No. 12, 1980, pp. 33-43.

4. D. A. Jones, B. E. Wilde, "Galvanic Reactions During Localized Corrosion on Stainless Steel," Corrosion Science, Vol. 18, 1978, pp. 631-643.

5. LLNL, 6-month exposure test, concentrated J-13, August 1997.

6. H. P. Hack, Crevice Corrosion Behavior of Molybdenum-Containing Stainless Steel in Seawater, Materials Performance Vol. 22, No. 6, 1983, pp. 24-30.

7. T. Shibata, T. Takeyama, "Stochastic Theory of Pitting Corrosion," Corrosion, Vol. 33, No. 7, 1977, pp. 243-251.

8. T. Shibata, "Statistical and Stochastic Approaches to Localized Corrosion," Corrosion, Vol. 52, No. 11, 1996, pp. 813.

9. G. A. Henshall, "Modeling Pitting Corrosion Damage of High-Level Radioactive-Waste Containers Using a Stochastic Approach," Journal of Nuclear Materials, Vol. 195, 1992, pp. 109-125.

10. G. A. Henshall, "Stochastic Modeling of the Influence of Environment on Pitting Corrosion Damage of Radioactive-Waste Containers," Materials Research Society Symposium, Vol. 353, 1995, pp. 679-686.

11. G. A. Henshall, "Modeling Pitting Degradation of Corrosion Resistant Alloys," Lawrence Livermore National Laboratory, University of California, UCRL-ID-125300, November 1996, 26 p.

12. J. W. Oldfield, W. H. Sutton, "Crevice Corrosion of Stainless Steels: I. A Mathematical Model," British Corrosion Journal, Vol. 13, No. 1, 1978, pp. 13-22.

13. F. A. Cotton, G. Wilkinson, Advanced Inorganic Chemistry, 5th Ed., John Wiley & Sons, New York, NY, 1988, pp. 679-755.

14. A. R. Hoch, A. Honda, F. M. Porter, S. M. Sharland, N. Taniguchi, "Development of Mathematical Models for Long-Term Prediction of Corrosion Behavior of Carbon Steel Overpacks for Radioactive Waste Containers," Mat. Res. Soc. Symp. Proc. Vol. 465, Materials Research Society, 1997, pp. 683-690.

15. J. S. Newman, Electrochemical Systems, 2nd Ed., Prentice Hall, Englewood Cliffs, NJ, 1991.

16. V. G. Jenson, G. V. Jeffreys, Mathematical Methods in Chemical Engineering, Academic Press, New York, NY, 1963, pp. 410-422.

17. D. D. McCracken, W. S. Dorn, Numerical Methods and Fortran Programming with Applications in Science and Engineering, John Wiley and Sons, New York, NY, 1964, pp. 377-385.

18. P. O. Gartland, "A Simple Model of Crevice Corrosion Propagation for Stainless Steels in Sea Water," Corrosion 97, Paper No. 417, National Association of Corrosion Engineers, Houston, TX, 1997, 17 p.

19. Y. Xu, H. W. Pickering, "The Initial Potential and Current Distributions of the Crevice Corrosion Process," J. Electrochemical Society, Vol. 140, No. 3, 1993, pp. 658-668.

20. E. A. Nystrom, J. B. Lee, A. A. Sagues, H. W. Pickering, "An Approach for Estimating Anodic Current Distributions in Crevice Corrosion from Potential Measurements," J. Electrochemical Society, Vol. 141, No. 2, 1994, pp. 358-361.

21. J. C. Farmer, G. E. Gdowski, R. D. McCright, H. S. Ahluwahlia, "Corrosion Models for Performance Assessment of High-Level Radioactive-Waste Containers," Nuclear Engineering Design, Vol. 129, 1991, pp. 57-88.

22. T. Okada, "Halide Nuclei Theory of Pit Initiation in Passive Metals, J. Electrochemical Society, Vol. 131, No. 2, 1984, pp. 241-247.

23. T. Okada, "A Theory of Perturbation-Initiated Pitting, Proceedings of the International Symposium Honoring Professor Marcel Pourbaix on his Eightieth Birthday: Equilibrium Diagrams and Localized Corrosion, R. P. Frankenthal, J. Kruger, Eds., Electrochemical Society, Pennington, NJ, Vol. 84-9, 1984, pp. 402-431.

24. C. Y. Chao, L. F. Lin, D. D. McDonald, "A Point Defect Model for Anodic Passive Films, II. Chemical Breakdown and Pit Initiation," J. Electrochemical Society, Vol. 128, No. 6, 1981, pp. 1194-1198.

25. N. Sato, Electrochimica Acta, Vol. 19, 1971, p. 1683.

26. H. W. Pickering, R. P. Frankenthal, "On the Mechanism of Localized Corrosion of Iron and Stainless Steel: I. Electrochemical Studies," J. Electrochemical Society, Vol. 119, No. 10, 1972, pp. 1297-1304.

27. J. R. Galvele, "Transport Processes and the Mechansim of Pitting of Metals," J. Electrochemical Society, Vol. 123, No. 4, 1976, pp. 464-474.

28. T. R. Beck, R. C. Alkire, "Occurrence of Salt Films During Initiation and Growth of Corrosion Pits," J. Electrochemical Society, Vol. 123, No. 4, 1976, pp. 464-474.

29. J. C. Farmer, "Crevice Corrosion and Pitting of High-Level Waste Containers: A First Step Towards the Integration of Deterministic and Probabilistic Models," Lawrence Livermore National Laboratory, University of California, UCRL-ID-128381, July 1997, 98 p.

30. H. -H. Strehblow, "Mechanisms of Pitting Corrosion," Chapt. 7, in Corrosion Mechanisms in Theory and Practice, P. Marcus, J. Oudar, Eds., Marcel Decker, New York, NY, 1995, pp. 201-237.

31. J. R. Scully, "Appendix D, Elicitation Interview Summaries," Waste Package Degradation Expert Elicitation Project Final Report, K. J. Coppersmith, R. C. Perman, M. Pendleton, J. L. Younker, Civilian Radioactive Waste Management System Management and Operating Contractor, Geomatrix Consultants, San Francisco, CA, August 15, 1997, pp. JS 1-30.

32. G. P. Marsh, K. J. Taylor, Z Sooi, "The Kinetics of Pitting Corrosion of Carbon Steel," SKB Technical Report 88-09, Swedish Nuclear Fuel and Waste Management Company (SKB), Box 5864, S-102 48, Stockholm, 1988, 39 p.

33. G. E. Gdowski, "Survey of Degradation Modes of Four Nickel-Chromium-Molybdenum Alloys," Lawrence Livermore National Laboratory, University of California, UCRL-ID-108330, March 1991, 67 p.

34. A. K. Roy, D. L. Fleming, B. Y. Lum, "Effect of Environmental Variables on Localized Corrosion of High-Performance Container Materials," Lawrence Livermore National Laboratory, University of California, UCRL-JC-125329, January 1997, 16 p.

35. A. K. Roy, D. L. Fleming, B. Y. Lum, "Localized Corrosion of Container Materials in Anticipated Repository Environments," Lawrence Livermore National Laboratory, University of California, UCRL-JC-122861, May 1996, 10 p.

36. A. K. Roy, D. L. Fleming, B. Y. Lum, "Electrochemical and Metallographic Evaluation of Alloy C-22 and 625," Lawrence Livermore National Laboratory, University of California, UCRL-ID-127355, May 1997, 10 p.

Table 1. Parameter Values Used in Probabilistic Pitting Model

Parameter	Units	Assumed Value
λ_0	min^{-1}	6.7572×10^{-2}
α_λ	none	0.5
E_{crit}	mV vs. SCE	+86
μ_0	min^{-1}	2.2137×10^{12}
α_μ	none	0.5
E_{pass}	mV vs. SCE	+1
γ_0	min^{-1}	5.0×10^{2}
A_γ	J $mole^{-1}$	3.0×10^{4}
τ_0	min	1.0
A_τ	J $mole^{-1}$	3.0×10^{4}
A	none	9.0
B	none	3.0
n	none	1.0
K_0	cm^2 L $mole^{-1}$ sec^{-1} V^{-1}	$4.4106\,540 \times 10^{-4}$

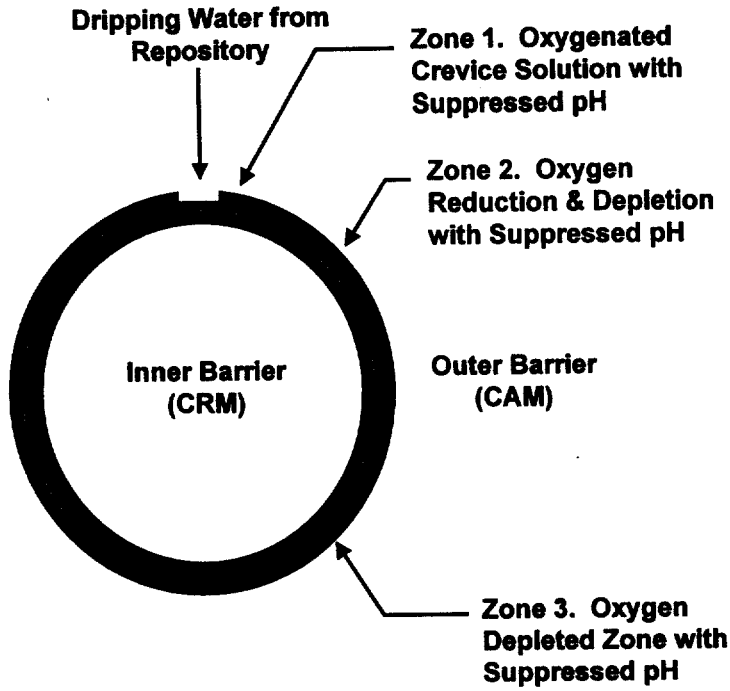

Figure 1. Conceptual representation of the waste package under attack. Illustration of crevice between CAM and CRM. Definition of Zones 1, 2 and 3.

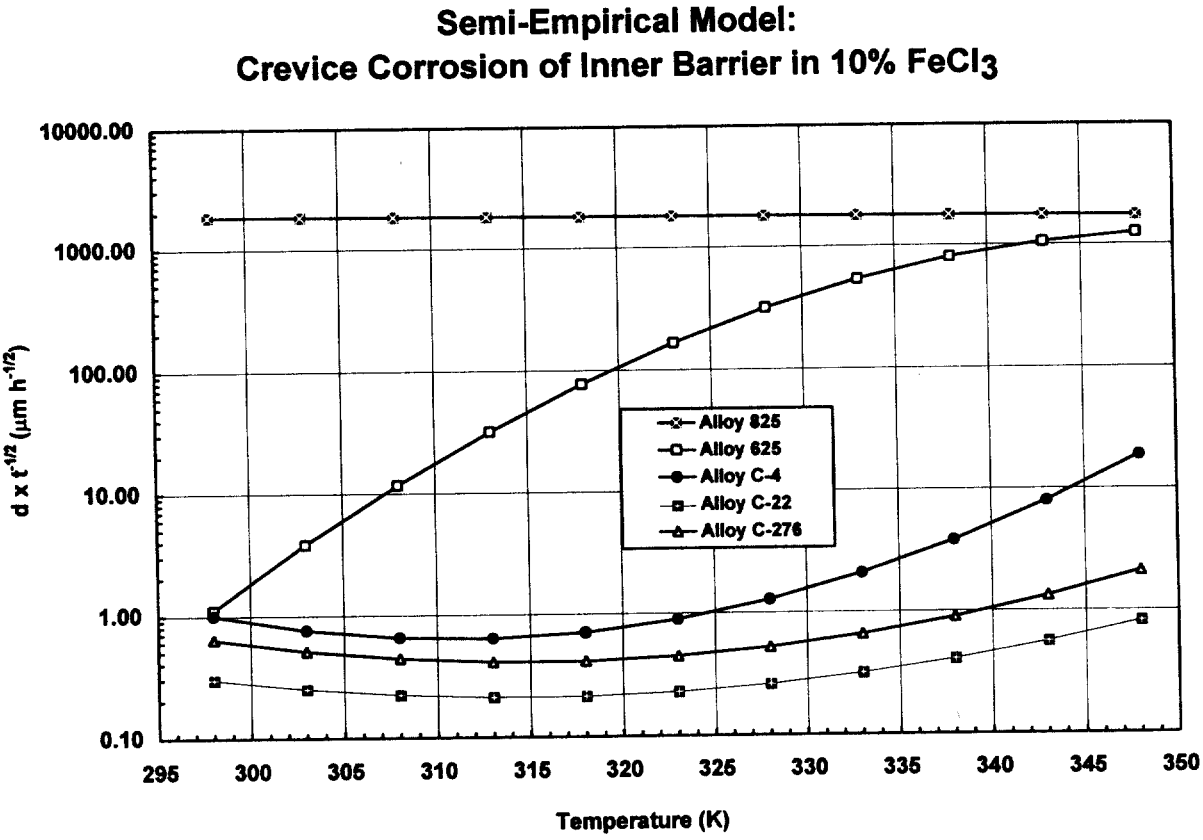

Figure 2. Empirical fit of the Sand equation to the experimental data of Asphahani for Alloys 825, 625, C-4, C-22 and C-276 exposed to 10 wt. % $FeCl_3$. A plot of d $t^{-1/2}$ verses temperature.

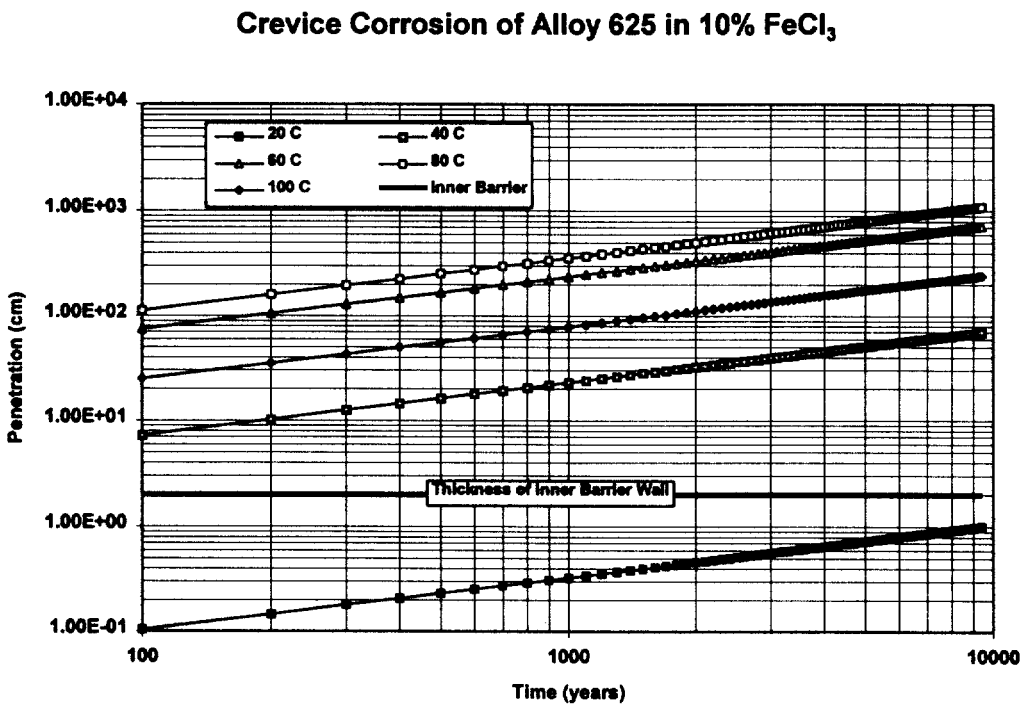

Figure 3. Predicted penetration of Alloys 625 at temperatures ranging from 20 to 100°C. The environment is assumed to be 10 wt. % $FeCl_3$.

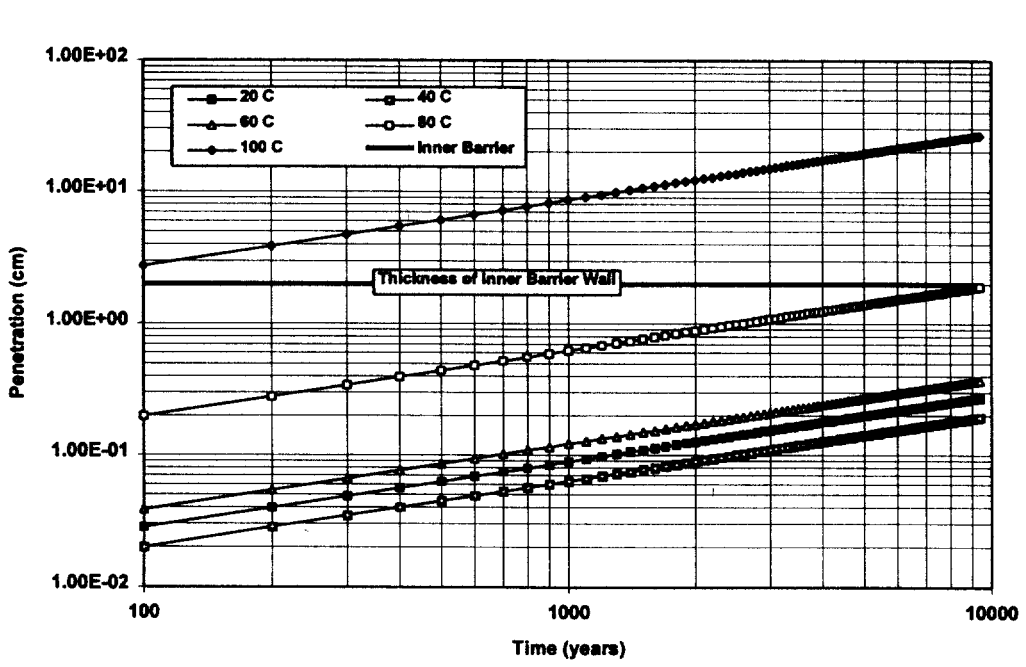

Figure 4. Predicted penetration of Alloys C-22 at temperatures ranging from 20 to 100°C. The environment is assumed to be 10 wt. % $FeCl_3$. No penetration is predicted for Alloy C-22 over 10,000 year period at temperatures ≤ 80°C.

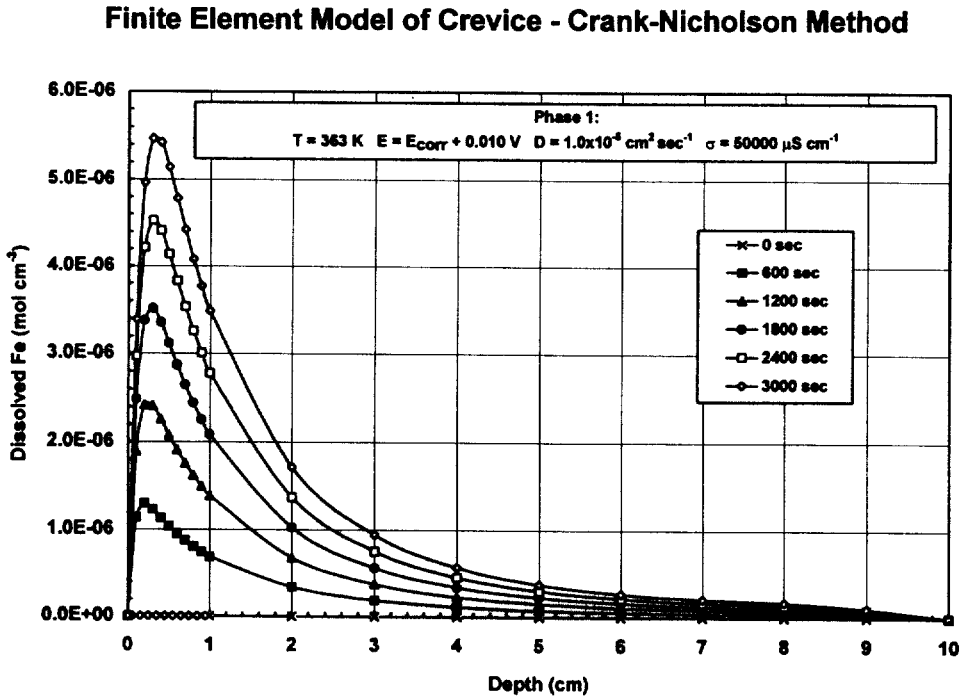

Figure 5. Finite-element model of the crevice during Phase 1. Transient concentration profiles for dissolved iron calculated with the Crank-Nicholson method.

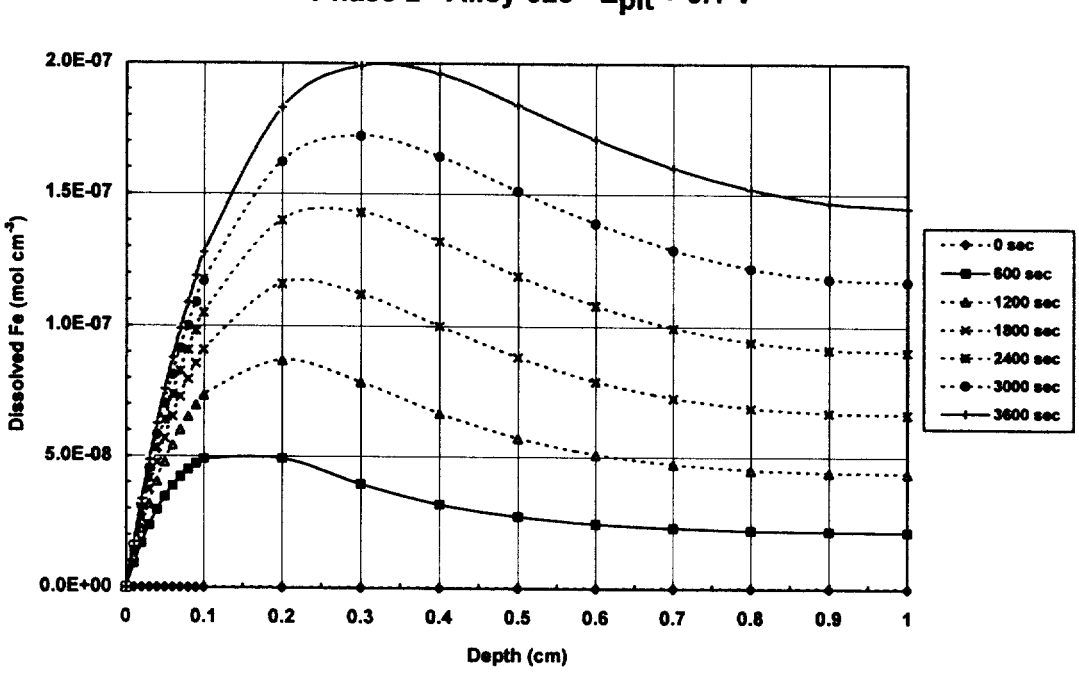

Figure 6. Transient concentration profiles of dissolved Fe predicted for Alloy 625 during Phase 2 crevice corrosion.

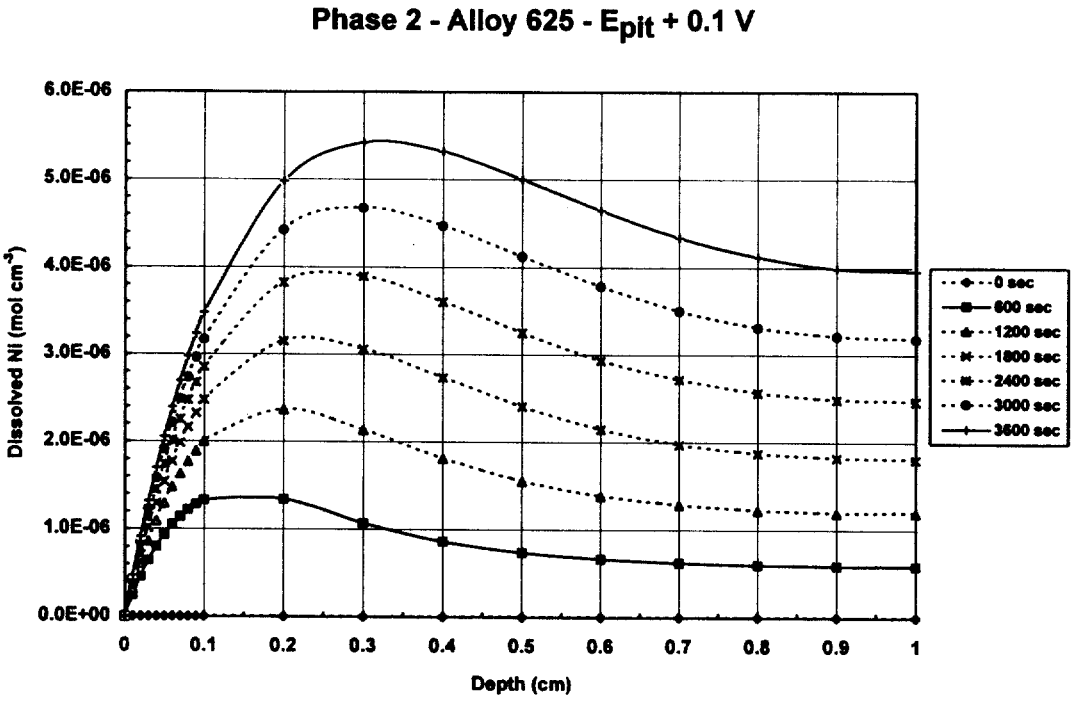

Figure 7. Transient concentration profiles of dissolved Ni predicted for Alloy 625 during Phase 2 crevice corrosion.

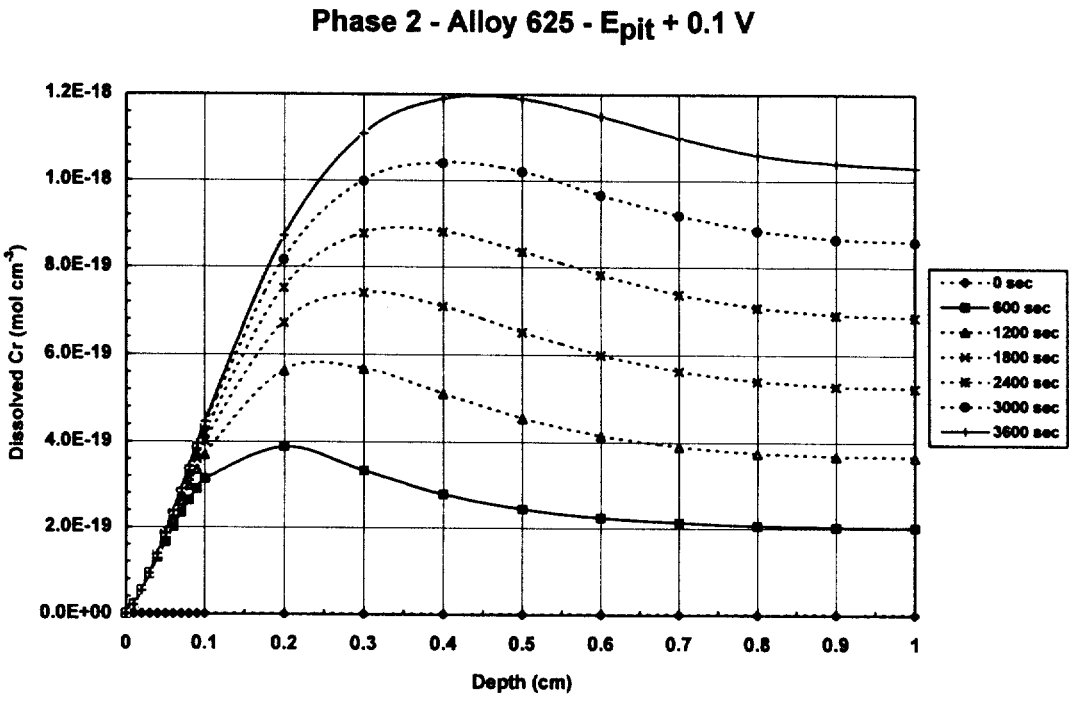

Figure 8. Transient concentration profiles of dissolved Cr predicted for Alloy 625 during Phase 2 crevice corrosion.

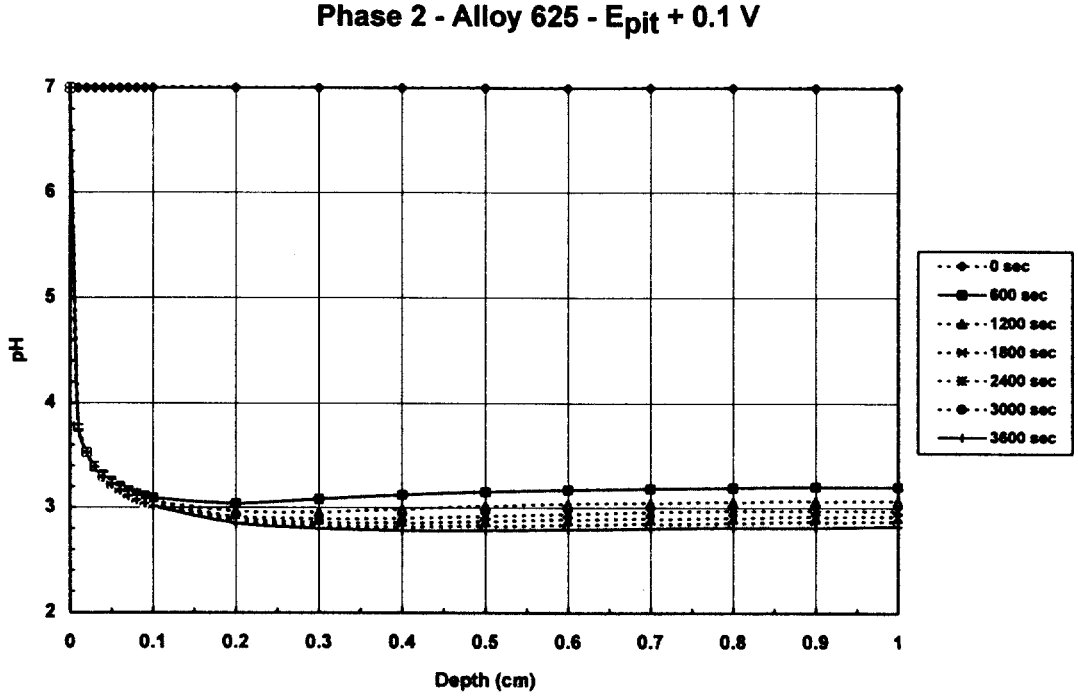

Figure 9. Transient pH profiles predicted for Alloy 625 during Phase 2 crevice corrosion.

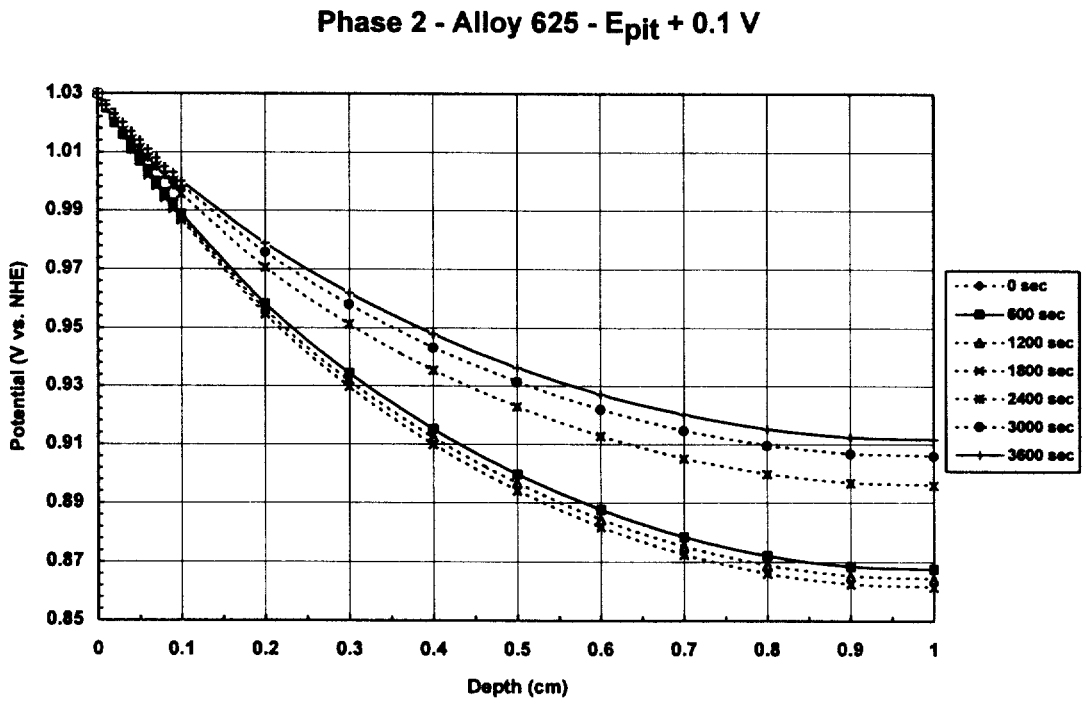

Figure 10. Potential profiles predicted for Alloy 625 during Phase 2 crevice corrosion.

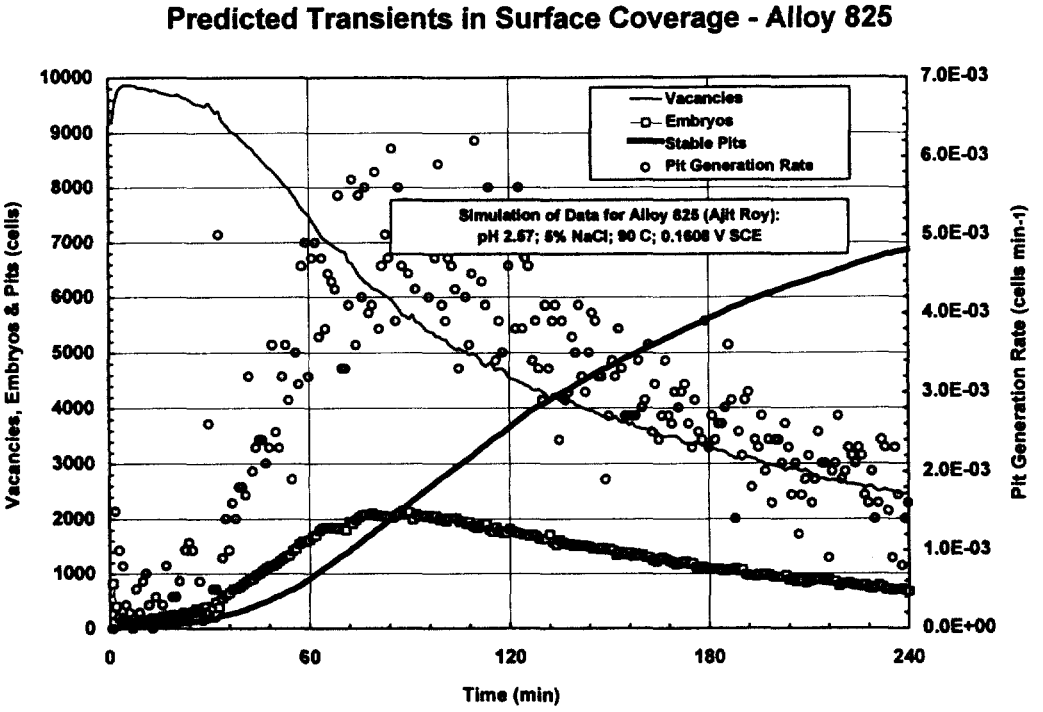

Figure 11. Transients in the density of vacancies, embryos and stable pits predicted for Alloy 825, based upon the probabilistic pitting model.

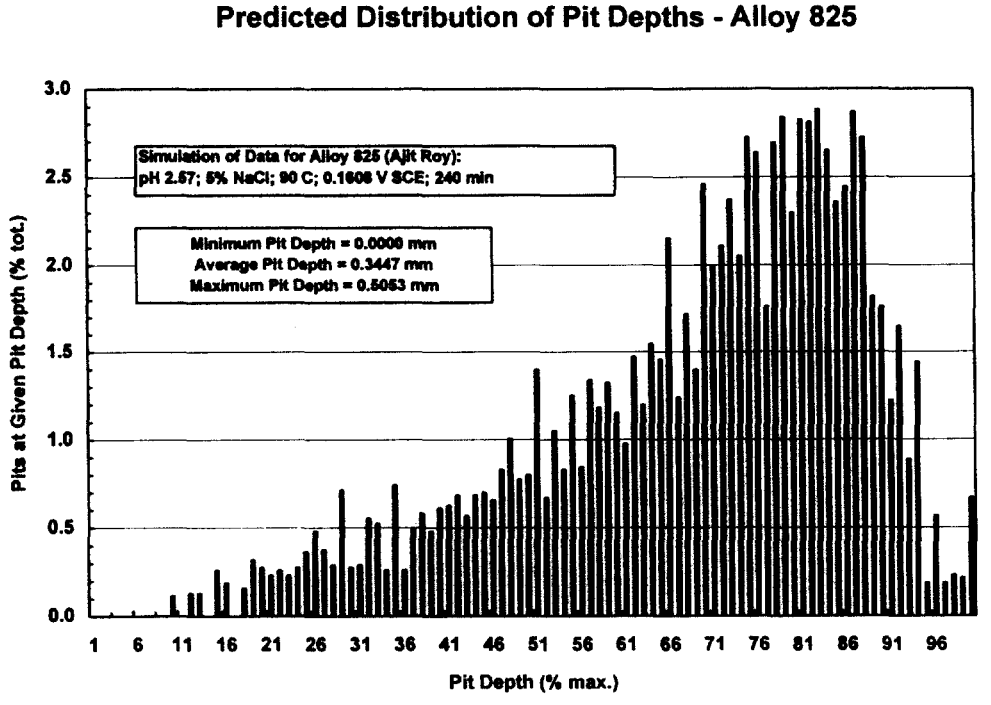

Figure 12. Distribution of pit depths predicted for Alloy 825, based upon the probabilistic pitting model.

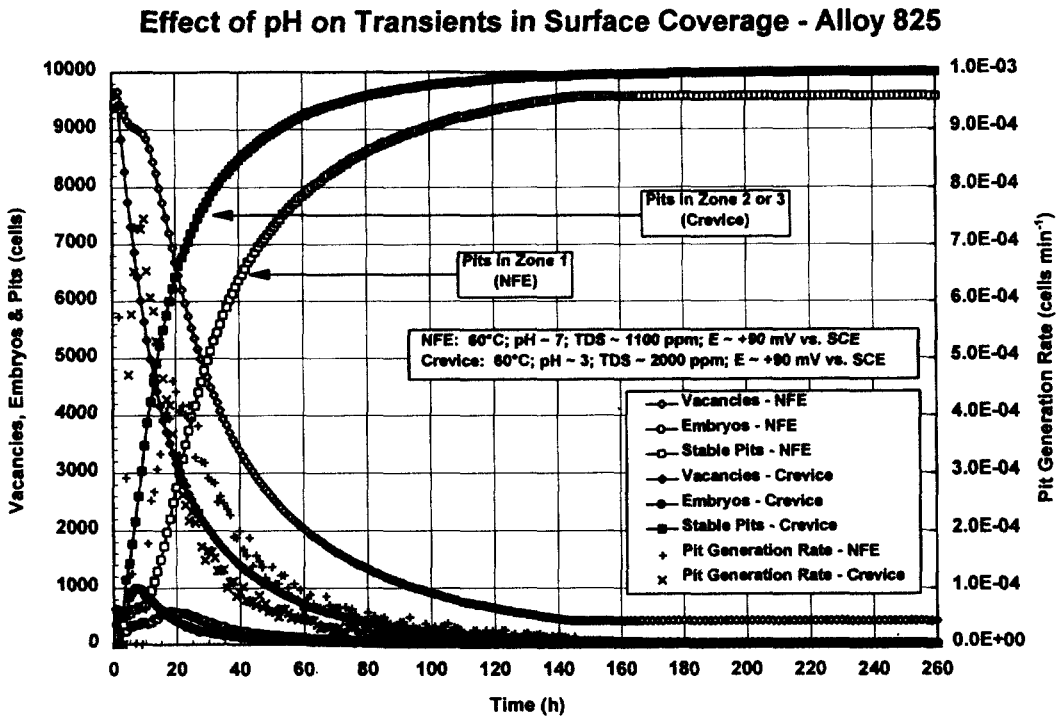

Figure 13. Effect of pH on the pitting of Alloy 825. Transients in the density of vacancies, embryos and stable pits initially predicted with the probabilistic pitting model. The material is assumed to be polarized at the pitting potential.

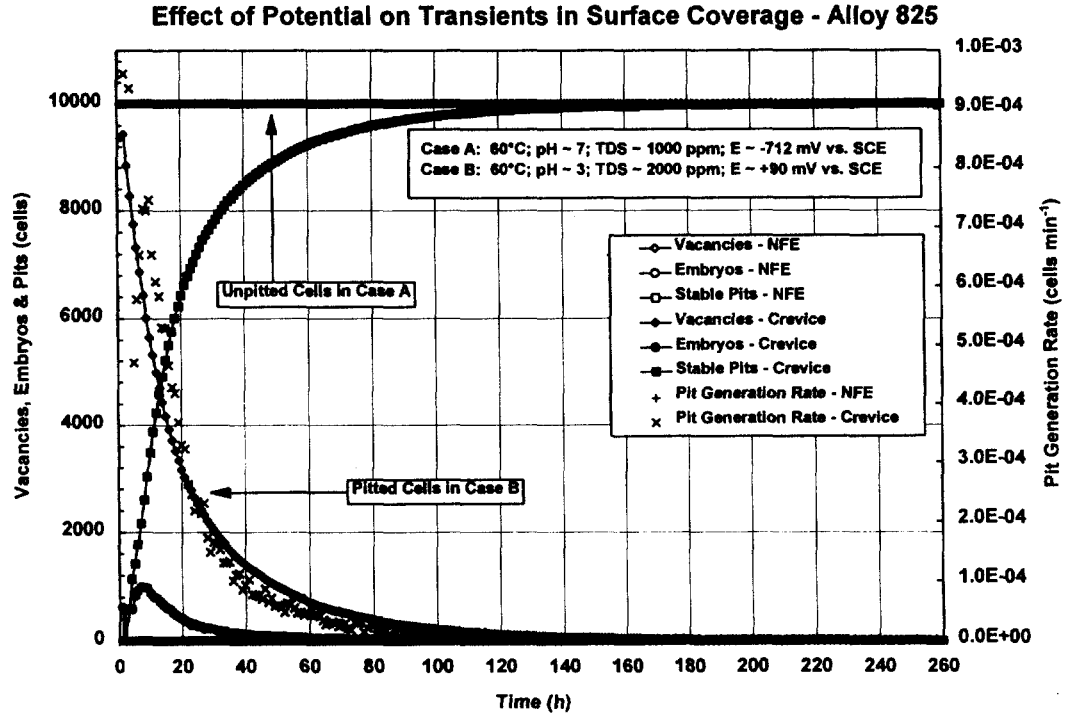

Figure 14. Effect of potential on the pitting of Alloy 825. Transients in the density of vacancies, embryos and stable pits predicted with the probabilistic pitting model.

Technical Information Department • **Lawrence Livermore National Laboratory**
University of California • Livermore, California 94551